KERNFORSCHUNGSANLAGE JÜLICH GmbH

Institut für Festkörperforschung

Neutron Scattering on Neutron Irradiated Steel

by

D. Schwahn, D. Pachur, and J. Schelten

Jül - 1543
Oktober 1978
ISSN 0366-0885

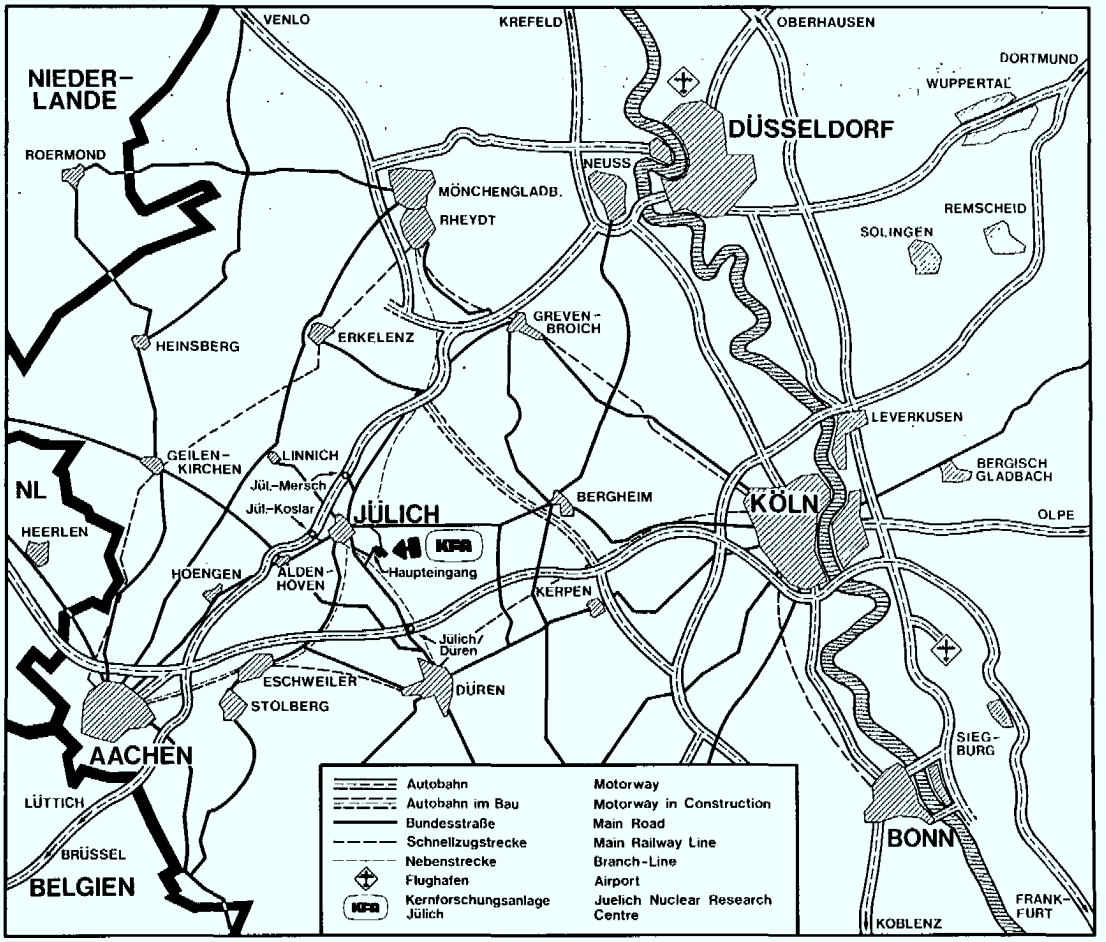

Als Manuskript gedruckt

Berichte der Kernforschungsanlage Jülich - Nr. 1543

Institut für Festkörperforschung Jül - 1543

Zu beziehen durch: ZENTRALBIBLIOTHEK der Kernforschungsanlage Jülich GmbH,
Jülich, Bundesrepublik Deutschland

Neutron Scattering on Neutron Irradiated Steel

by

D. Schwahn*, D. Pachur and J. Schelten***

* Institut für Festkörperforschung

** Zentralabteilung Brennelement- und Bestrahlungstechnologie

Zusammenfassung

Drei Reaktordruckbehälterstähle (zwei Grundmaterialien und ein Schweißgutmaterial) mit einer relativen strahleninduzierten Härtezunahme von 50 % wurden mit der Neutronenkleinwinkelstreuung untersucht. Alle drei Systeme wurden im leichtwasser-moderierten Forschungsreaktor FRJ-1 bei einer Temperatur von 150°C bestrahlt. Beim Grundmaterial A, einem Reaktordruckbehälterstahl gemäß ASTM A 533 B, zeigte sich der stärkste Streueffekt. Dieses System war mit einer Neutronenfluenz von $7\ 10^{19}$ n/cm^2 (E > 1 MeV) bestrahlt worden. Es wurde an diesem System das Ausheilverhalten verfolgt, indem isochron (4 Stunden) bei 300, 350, 400 und 450°C ausgeheilt wurde. Parallel zu den Neutronenstreumessungen wurde an den Proben die Härte gemessen. Die Härtezunahme von 50 % hat nach dem ersten Ausheilschritt auf 30 % und nach dem zweiten auf 18 % abgenommen. Die entsprechenden Neutronenstreuspektren zeigen eine Abnahme von sehr kleinen Poren mit Guinierradien von höchstens 5 Å, die ausheilten oder sich zu größeren Poren (R_g = 20-25 Å) mit einer Dichte von $n = 10^{15}$ cm^{-3} zusammenlagerten. Nach dem dritten Ausheilschritt bei 400°C sind die Streukurven innerhalb der statistischen Genauigkeit mit denen der unbestrahlten Referenzprobe identisch; die gemessene Härtezunahme betrug jedoch noch 13 %.

Stahl B und das Schweißgut zeigte vor der Ausheilung qualitativ dasselbe Streubild wie Stahl A. Am Schweißgutmaterial, das mit einer Neutronenfluenz von $5\ 10^{19}$ n/cm^2, E > 1 MeV, bestrahlt war, wurde das Ausheilverhalten noch nicht im Neutronenstreuexperiment untersucht. Im Stahl B, der einen Vanadiumgehalt von 0,2 gew.% hat und mit einer Neutronenfluenz von $1,5\ 10^{19}$ n/cm^2 (E > 1 MeV) bestrahlt worden war, wurden nach Ausheilung (Härtezunahme von 50 % aud 32 %) keine Poren mit Durchmessern größer als 20 Å gemessen.

Abstract

Three pressure vessel steel systems (two base material and one weld material) with a 50 % irradiation induced hardness enhancement were investigated by small angle neutron scattering. All three steel systems were irradiated in the light water moderated research reactor FRJ-1 at a temperature of 150°C. The strongest scattering effect was found for steel A; a pressure vessel containment steel ASTM A 533 B. This system was irradiated with a fluence of 7 10^{19} n/cm^2 (E > 1 MeV). The annealing behaviour was then investigated after isochronal anneals of 300, 350, 400, and 450°C. Vicker's hardness measurements were made parallel to the neutron scattering experiments. The hardness enhancement of 50 % decreased after the first anneal to 30 % and after the second to 18 %. The neutron scattering patterns show a decrease in the number of very small voids having a Guinier radius less than 5 Å. These voids have annealed, or coagulated into larger voids (R_g = 20-25 Å) with a density of n = 10^{15} cm^{-3}. After the third anneal at 400°C, the scattering patterns became, within statistical errors, identical to the scattering pattern of the unirradiated specimen; but a hardness enhancement of 13 % was measured.

Prior the anneals, steel B and the weld material showed qualitatively the same scattering pattern as steel A. The annealing behaviour of the weld material, which was irradiated with a neutron fluence of 5 10^{19} n/cm^2, E > 1 MeV, has not yet been experimentally investigated by neutron scattering. In steel B, which has a vanadium content of 0.2 wt. % and was irradiated with a neutron fluence of 1.5 10^{19} n/cm^2 (E > 1 MeV), no voids larger than 20 Å in diameter were found after annealing (the hardness enhancement decreased from 50 % to 32 %).

Contents

1. Introduction

The material properties of the pressure vessel in a light water reactor are gradually changed by impinging high energy neutrons. The material becomes brittle, as is seen by ductility, strength, and hardness measurements, and therefore a certain time exists at which the safety standards specified for the vessel are no longer met. In power reactors the brittleness of the wall material is monitored by using surveillance specimens. These specimens are irradiated at a position inside the containment, near the core. In predetermined time intervals, some of these specimens are taken for testing mechanical-technological properties. The embrittlement of the reactor pressure vessel steel is determined by extrapolating the results obtained for these specimens. From this, it is found whether or not the reliability of the containment can still be warranted. This kind of extrapolation and therefore the critical examination of reactor reliability is much more powerful if one knows the factors influencing the embrittlement.

In nuclear power plants and material testing reactors, investigation programmes are carried out which show that parameters influencing embrittlement include: Alloy composition, trace element concentrations, microstructure, applied stress, irradiation temperature, fluence and spectrum of neutrons. Obviously, embrittlement is a very complex mechanism since it is effected by many different factors. A detailed knowledge of this mechanism would require a large number of experiments needing a prohibitively long time and costing a large amount of money. A reduction in the number of these experiments, without loosing any information, is only possible if the embrittlement mechanism is understood better. This is feasible if one knows the microscopic behaviour during irradiation and annealing and if its correlation with the mechanical-technological properties is understood.

Therefore, it is our opinion that these mechanical tests ought to be coupled with microscopic methods, e.g. with transmission electron microscopy (TEM), which is known to be an excellent

tool for investigating qualitatively radiation defects such as dislocation loops and voids. However, a tedious preparation of the radioactive specimens is required and therefore only a limited amount of specimens can only be investigated by TEM. Based on many years of fundamental research in elastic neutron scattering, it can be predicted that neutron scattering is a valuable method for obtaining quantitative information on the changes of the microstructure owing to neutron irradiation. A first attempt to determine void parameters in neutron irradiated steel using a neutron scattering technique was made in Geesthacht by Frisius and Naraghi (1977). It is this method which should be coupled with the well established mechanical test procedures in order to give a better understanding of the changes in the mechanical properties produced by changes in the microstructure. Small angle neutron technique satisfies the following requirements:

1. Neutron scattering is a non-destructive method, i.e. a scattering experiment can be repeated with the same specimen as often as necessary.

2. The sample properties are not changed by neutron scattering.

3. The measured scattering pattern is a bulk-averaged quantity.

4. The interpretation of the scattering pattern is understood well.

5. Nowadays, the measurement time can be kept within tolerable limits.

It is the purpose of this paper to report on small angle neutron scattering experiments with various steel samples which have been irradiated with neutron fluences between 10^{18} and 10^{19} ncm^{-2} ($E > 1$ MeV) and then isochronally annealed. Irradiation-induced neutron scattering is observed which is quantitatively interpreted in terms of void parameters and dislocation loop parameters. Annealing causes these parameters to change significantly. An attempt is made to correlate these scattering data with changes in the measured hardness of the

same specimen. The aim of this study was to demonstrate the feasibility of obtaining irradiation-induced microstructure changes in pressure vessel steel samples.

2. Mechanical Testing of Irradiated Steel

Investigations of the annealing behaviour of irradiation induced damage show that processes of different activation energy occur (Pachur, 1976). These processes were investigated by measuring the Vickers hardness, a test which requires only a few specimens and is simple to carry out. Furthermore, it was found as a result of various irradiation programmes that the relative enhancement of the irradiation induced hardness is proportional to the enhancement of the NDT (nil-ductility temperature) measured in impact tests. Therefore, it appears that the enhancement of hardness and of NDT are caused by similar irradiation induced defects. The irradiation induced tensile strength increment has a somewhat different behaviour. Processes having the highest activation energy, as observed in hardness measurements, do not occur. This means that the tensile strength increment vanishes at a relatively low annealing temperature.

The number of annealing processes changes for different irradiation temperatures. For an irradiation at 150°C, up to five separate processes were observed depending on the system; while for irradiation temperatures at 300°C and higher, the number of annealing processes decreased. The anneal of the irradiation induced defects starts above 215°C. For the neutron small angle scattering experiments, samples irradiated at 150°C were selected in order to have pure irradiation defects.

2.1 Characterization of the Specimens

Three different systems were examined in the neutron experiments; their composition analysis is given in Tab. 2.1.

Stahl	% C	% Si	% Mn	% P	% S	% N	% Al	% B	% Co	% Cr	% Cu	% Mo	% Ni	% V
Grundwerkstoff A	0,22	0,30	1,44	0,012	0,008	0,023	0,023	<0,0005	0,01	0,12	0,12	0,51	0,63	0,01
Grundwerkstoff B	0,11	0,35	1,36	0,012	0,008	0,016	0,014	<0,001	0,013	0,11	0,11	0,37	1,50	0,15
Schweißgut	0,06	0,21	1,85	0,012	0,003	0,011	0,015	0,0003	0,023	0,08	0,29	0,56	1,30	0,02

Tab. 2.1 Composition analysis of the steel systems in wt %.

From the data in Tab. 2.1, the differences between the systems can be seen. Steel A is the normal reactor pressure steel containment material ASTM A533B. Specimens from one block of this system were irradiated under different conditions and were then investigated by different testing procedures (Pachur, 1974). These experiments are co-ordinated by an IAEA-irradiation programme. Steel B contents much more vanadium and somewhat more nickel than steel A. The heat treatment of both steel systems was the same (Pachur and Sievers, 1975). The third system is a weld material which has a high copper content of 0.29 wt %. This high copper concentration seems to be responsible for the strong sensitivity of this system to irradiation.

2.2 Irradiation Procedure

The specimens were irradiated for different times at the same incore position in the light water moderated FRJ-1 reactor. To ensure that processes of high activation energy take place, the specimens must be irradiated for a minimum length of time. For the neutron experiments, specimens were selected having nearly the same amount of damage, i.e. 50 % enhancement of hardness. This enhancement of hardness is produced in steel A by a neutron fluence of $7\ 10^{19}$ n/cm^2, E > 1 MeV, in steel B by $1.5\ 10^{19}$ n/cm^2, E > 1 MeV and in weld material by a neutron fluence of $5\ 10^{19}$ n/cm^2, E > 1 MeV. The results of the mechanical testing are given in Tab. 2.2.

Research Reactor FRJ-1, H_2O-moderated, Irradiation Temperature 150°C						
	Steel A		Steel B		Weld material	
Neutron Fluence E > 1 MeV	unirradiated	7×10^{19} n/cm^2	unirradiated	$1{,}5 \times 10^{19}$ n/cm^2	unirradiated	5×10^{19} n/cm^2
Block and Plate No.	L/S	LF				
0,2% yield strength $\sigma_{0,2}$ N/ncm^2	500	895	504	845	610	
ultimate tensile strength σ_u N/ncm^2	624	895	632	845	745	
yield point ratio $\sigma_{0,2} / \sigma_u$ {%}	0.8	1	0.8	1	0.82	
Elongation δ {%}	23	4.9	27.7	11	20	
Reduction of Area Ψ {%}	68	58	72.7	65	65	
Vickers Hardness HV10 N/ncm^2	2000	2980	1835	2806	2220	3440
Transition Temperature TT, 30ft-Lb ≙ 51 J/cm^2	25°C	145°C	- 12°C	110°C	- 32°C	
Increase of Transition Temperature ΔT_T		120°C	-	122°C	-	
Upper Shelf Energy J/cm^2	157	128	220	166	157	
Remarks					weld material was investigated at irradiation temperatures of 300 and 400°C.	

Tab. 2.2 Results of mechanical testing.

2.3 Annealing Procedure

Specimens from the same block were used for both the mechanical tests and the small angle neutron scattering measurements. For the neutron experiments, one half of a specimen, which was tested earlier in an impact test below room temperature, was used. The appearance of various processes during the anneal makes it reasonable to correlate them with different kinds of microstructure changes. For the neutron experiments, the specimens were heat treated in the same manner as for the hardness investigations. After each anneal Vickers hardness was controlled. The annealing curves for all three systems are shown in Fig. 2.1; each annealing procedure took 4 hours. From the behaviour of these curves, the annealing temperatures for the neutron experiment were determined to 300^{o}C, 350^{o}C, 400^{o}C, and 450^{o}C.

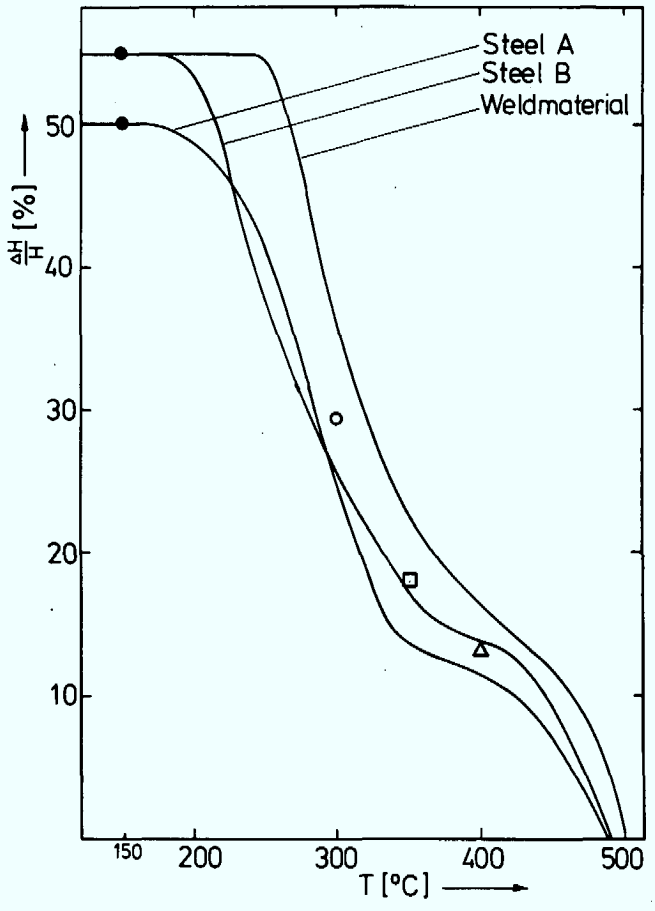

Fig. 2.1 Anneal of the enhancement of hardness as a function of temperature.

3. Experimental Aspects of Neutron Scattering

3.1 Neutron Small Angle Spectrometer

The neutron scattering experiments on the steel specimens were performed using the small angle neutron scattering spectrometer in the external laboratory of the FRJ-2 in Jülich. During the last eight years this instrument has been used to investigate the flux lines in type-II superconductors, the molecular configuration of solid polymers, the superparamagnetic behaviour in metals, the structure of precipitates and short-range order in alloys. This instrument is described by Schelten (1972) in detail. The neutrons are produced in the reactor, moderated in the cold source, and guided to the external laboratory by a curved total reflecting nickel coated glass channel. The neutrons are monochromated by a velocity selector and collimated by two cadmium apertures. Neutron guides of various lengths can be inserted between the velocity selector and the sample position in order to vary the collimation. In this way the neutron intensity at the sample and the resolution can be optimized for the experimental conditions. The neutrons scattered

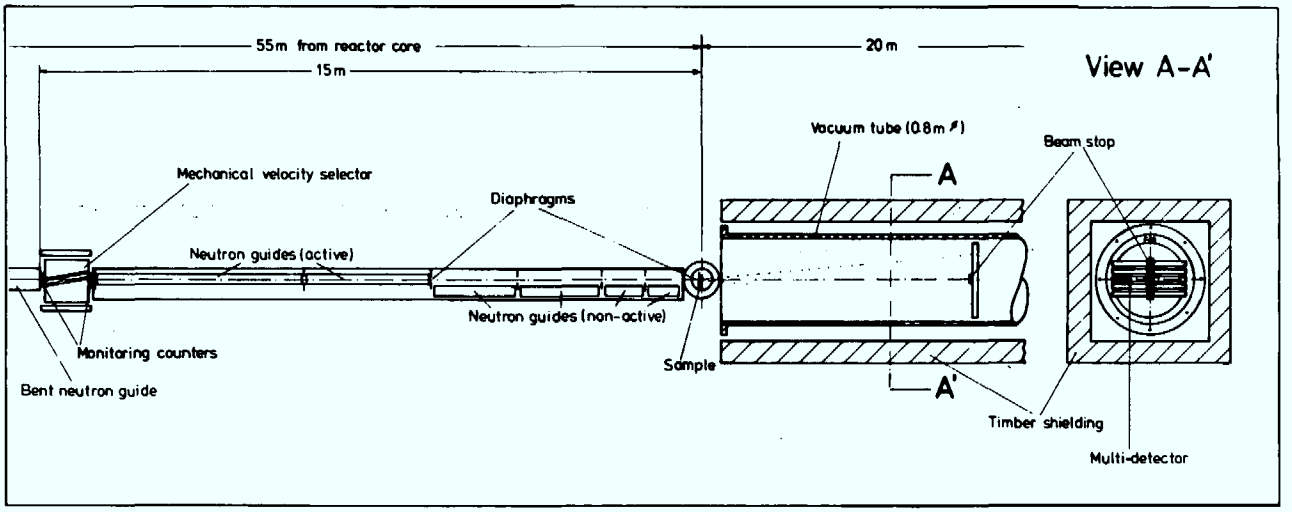

Fig. 3.1 Neutron small angle scattering apparatus at FRJ-2 in Jülich.

by the sample to small angles are detected by a position sensitive detector. Scattering angles between 0.2 and 12 degrees can be obtained by changing the sample-detector distance continuously. The unscattered neutron beam, which is usually much more intense than the scattered one, is absorbed by a piece of cadmium in front of the detector.

3.2 Specimen Container

Owing to their high radioactivity (0.04 Curie) the specimens could not be directly handled. Consequently, they were transported and measured in a specially prepared block of lead with a wall thickness of 6 cm. This made the transport of the specimens between the hot cells and the measuring place easier. The lead block contained seven horizontal holes. One hole, which was perpendicular to the neutron beam, contained the specimens. The other six holes were at the same height as the first but parallel to the neutron beam, which could freely penetrate the specimen through these holes. The lead block was fixed and calibrated on a moveable platform. It was necessary to transport the specimens several times to the hot cells and back again for annealing. The annealing was carried out in the same ofen, which was used for annealing the specimens, whose mechanical properties were tested.

A magnetic field could not be applied to saturate the ferromagnetic specimens. In such a saturation field, one can separate nuclear and magnetic neutron scattering (Schmatz et al., 1974). Also the intense scattering from Bloch walls and magnetic domains can be avoided. The measurements could not be done in a magnetic field because at the specimen position there is neither space for a 2 Tesla-magnet and the necessary lead shielding nor is the platform in the external laboratory strong enough to support such a weight.

3.3 Measured Scattering Curves

It came to light during the experiment that the scattered intensity corresponding to the largest possible scattering angles combined with incoming neutrons of the smallest possible wavelength (λ = 6.2 Å) had to be measured in order to obtain information about the system. For a statistical accuracy of 2-3 %, measuring times of 30 hours per spectrum were necessary.

All the measurements taken are plotted in Figs. 3.2-3.4. The macroscopic scattering cross-section (per cm^3 unit volume), which is proportional to the scattered intensity, is plotted in absolute units as a function of the momentum transfer κ.

$$\kappa = \frac{4\pi}{\lambda} \sin \delta/2 \qquad (3.1)$$

λ is the wavelength of the incident neutron beam and δ is the scattering angle.

Steel has a very complicated and heterogenious structure since precipitates and magnetic domains are present which cause neutrons to be scattered at small angles. Knowledge about the change of microstructure induced by the irradiation process can be obtained by comparing the curves for the irradiated and unirradiated specimens. This comparison assumes that specimens from the same block have the same scattering pattern. This could be proved by comparing the scattering pattern of the unirradiated with the annealed specimen in Fig. 3.2b.

The curves for the unirradiated samples are denoted by full squares (- ■ -) in all plots. The scattering curves of steel A (- ● -) show the strongest change caused by irradiation (Fig. 3.2a). This sample was annealed isochronally (4 hours) at various temperatures to study the change of microstructure. A strong change in the scattering pattern after the first anneal at 300°C was observed (Fig. 3.2 - o -); the intensity enhances by a factor of 2-3 at smaller κ-values. Qualitatively, this means that the scattering centres produced during irradiation cogulate during annealing. The scattering intensity decreased during the second anneal at 350°C (- □ -) (Fig. 3.2a) and

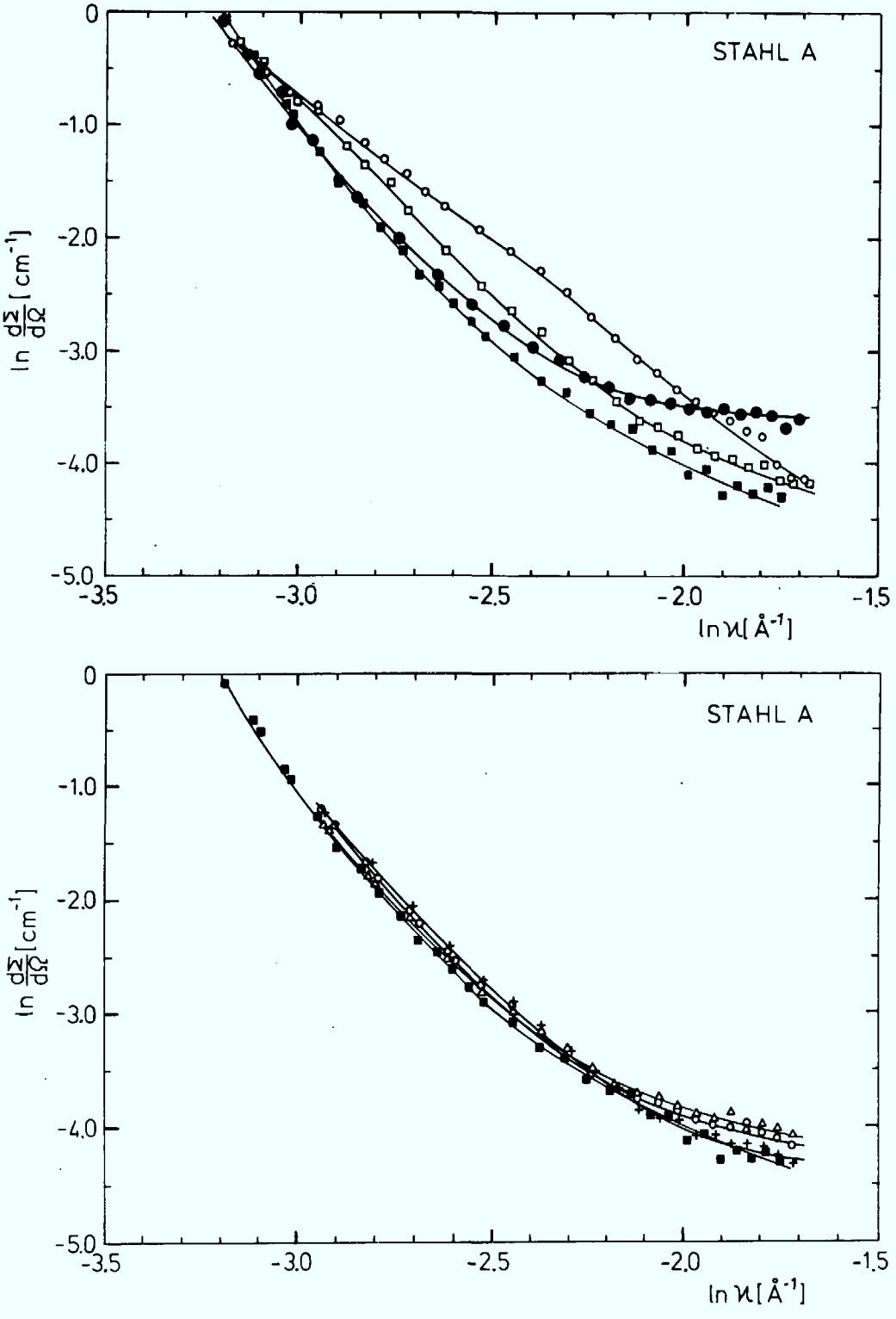

Fig. 3.2a/b Spectra of steel A in the large κ-range: - ■ - unirradiated specimen, - ● - irradiated specimen, - o - after first anneal at 300°C, - □ - after second anneal at 350°C, - Δ - after third anneal at 400°C, - + - after fourth anneal at 450°C (the symbols in all figures have the same meaning).

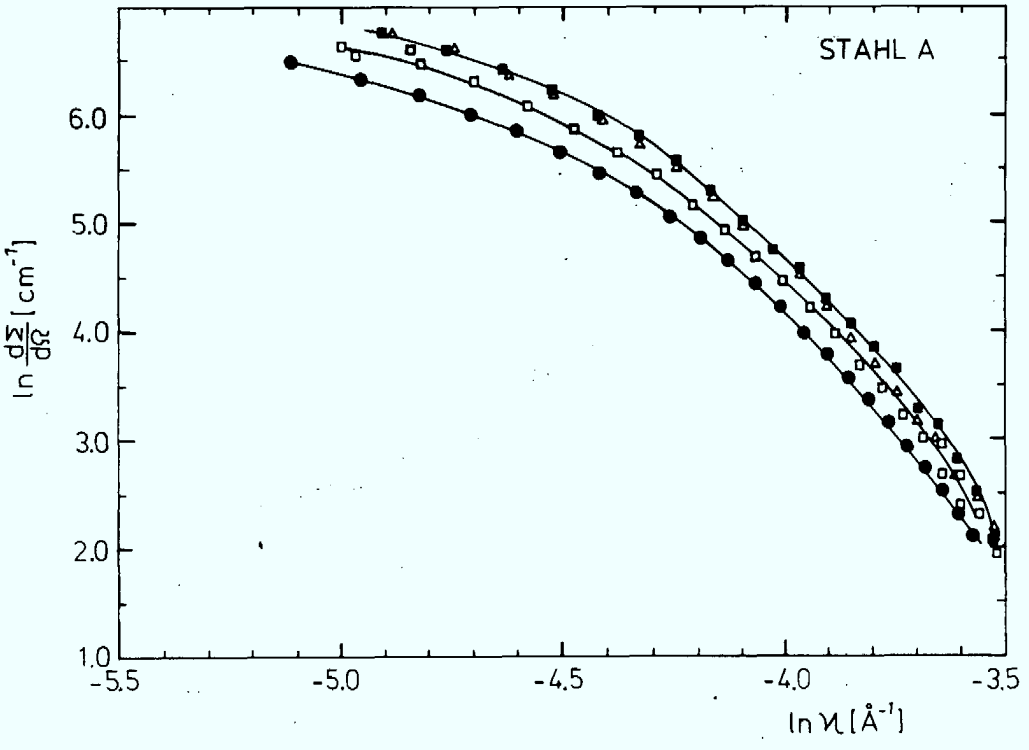

Fig. 3.2c Spectra of steel A in the small κ-range: In contrast to the large κ-range, the intensity of the irradiated specimen (- ● -) decreases relative to the unirradiated specimen (- ■ -). After the third anneal (- Δ -) the intensity of the irradiated specimen is again the same as the unirradiated one.

after the third anneal at 400°C (Fig. 3.2b) is virtually identical to the scattering pattern of the unirradiated specimen.

The irradiation induced enhancement in intensity was expected for the total κ-range since new scattering centers such as dislocation loops and voids are produced. But it is strange that the scattering intensity at very small angles (Fig. 3.2c) decreases instead of increasing. Furthermore, after the final anneal its shape is nearly identical to that of the unirradiated specimen. The decrease of the scattering at smallest κ-values appears to be caused by the correlation between the Bloch walls and the induced nonmagnetic irradiation damage. This can only be investigated by further neutron experiments in a magnetic saturation field.

The scattering effect of steel B was much weaker. The steel B specimen was irradiated with a fluence of $\phi = 10^{19}$ ncm^{-2} which is one order of magnitude smaller than that for steel A. Unlike steel A, the scattered intensity in the smallest κ-range (Fig. 3.3b) after annealing is larger than in the case of the unirradiated specimen. From this it has to be concluded that there are density fluctuations of long range order (100 Å), whose character cannot be explained by this measurement.

In the weld steel sample a similar effect was found as in steel A. No annealing experiments were performed on this system.

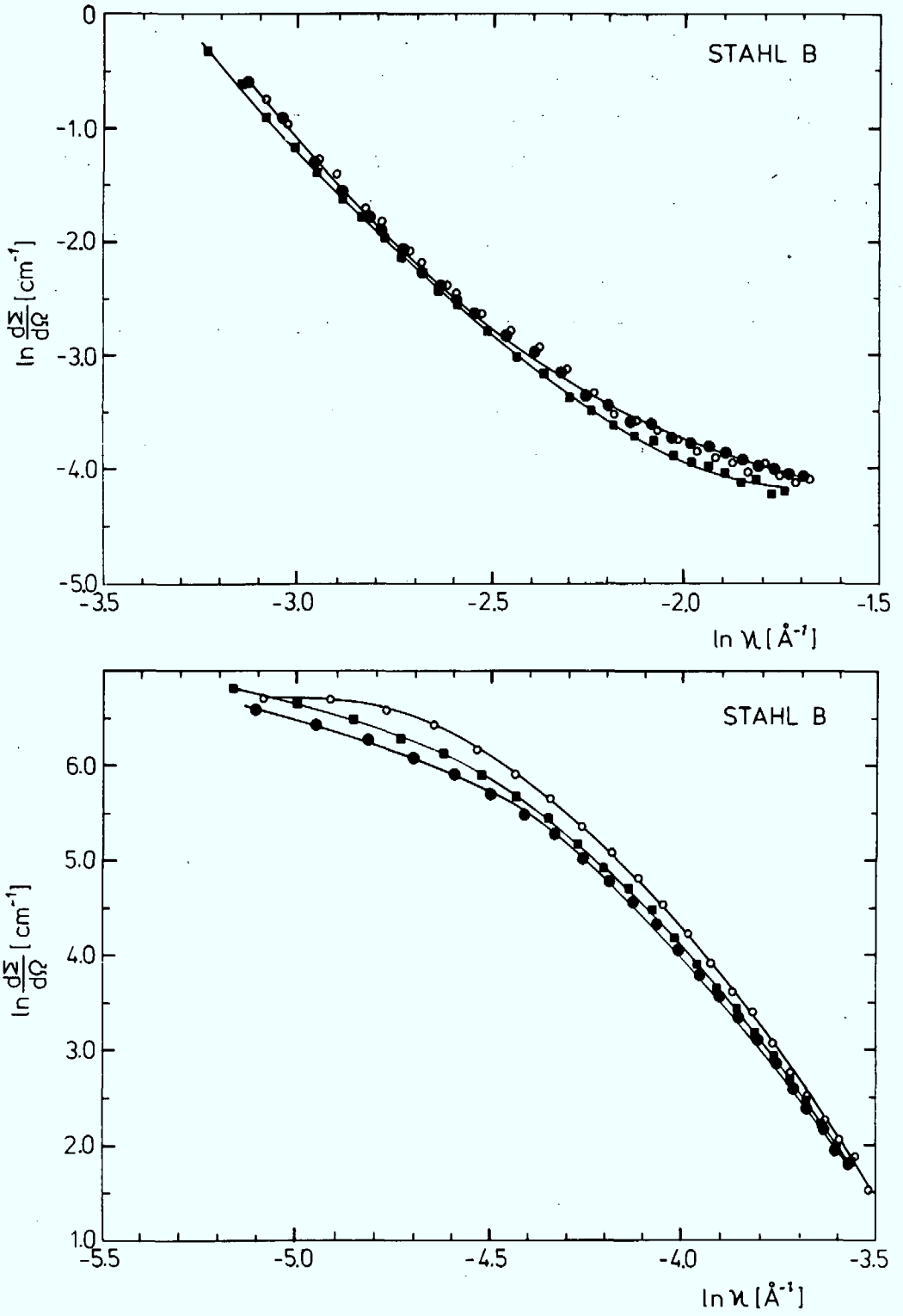

Fig. 3.3a/b Spectra of steel B in the large and small κ-range: For this system only a small change in intensity could be observed (meaning of symbols see text of Figs. 3.2a/b).

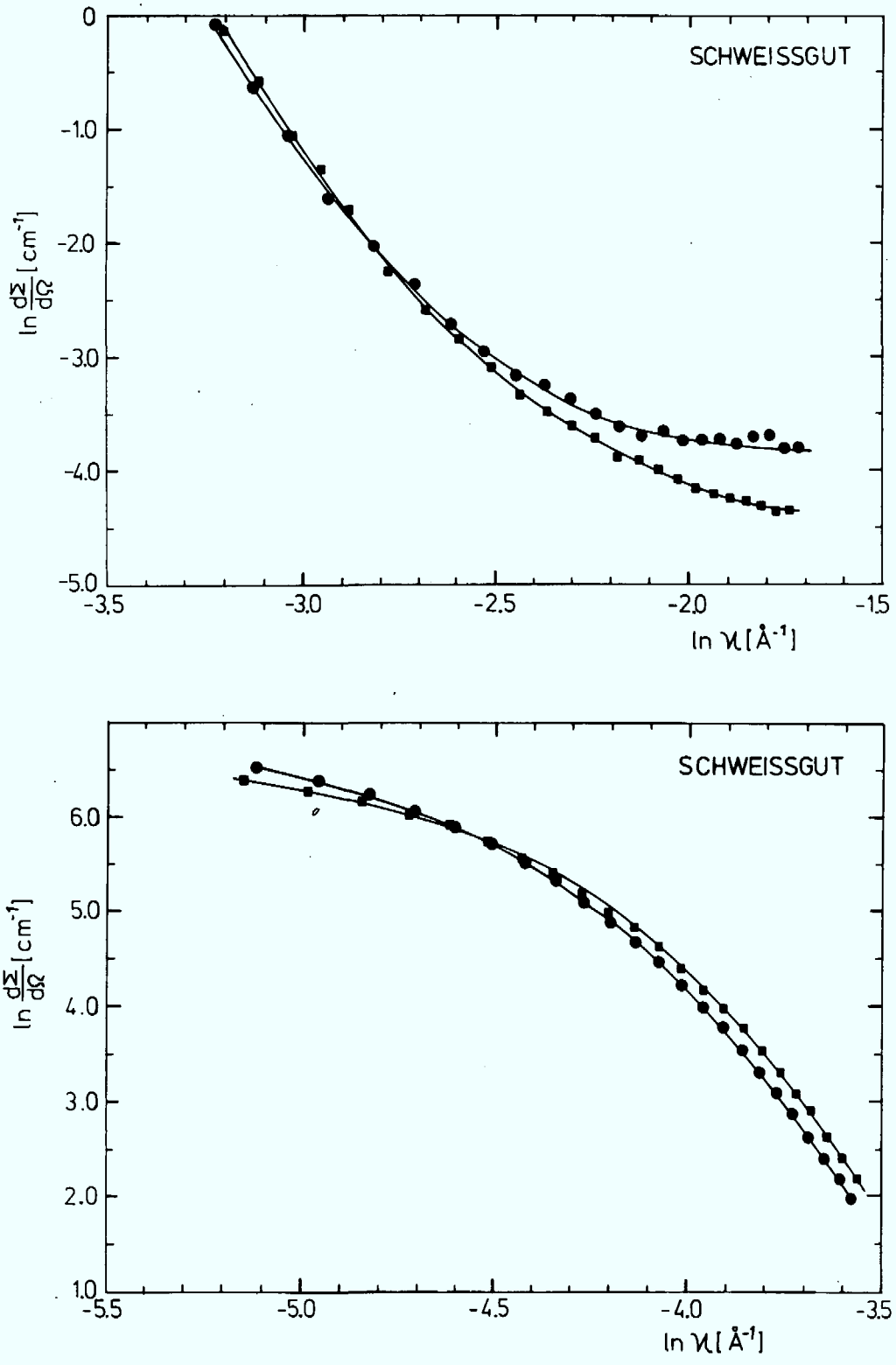

Fig. 3.4a/b Spectra of weld material in the large and small κ-range: In the large κ-range the same qualitative effect was found as in steel A (symbols see text in Figs. 3.2a/b).

4. Analysis of the Neutron Spectra

4.1 Scattering Theory

The elastic differential cross-section is given by

$$\frac{d\Sigma}{d\Omega}(\underline{\kappa}) = \frac{1}{V_S} \left| \int_{V_S} d\underline{r} \; (\rho(\underline{r}) - \bar{\rho}) \; e^{i\underline{\kappa}\underline{r}} \right|^2 \qquad (4.1)$$

(Schmatz et al., 1974, Guinier and Fournet, 1955). V_s is the volume of the sample, $\rho(\underline{r})$ the local scattering length density, and $\bar{\rho}$ the scattering length density averaged over the sample volume. The scattering length density is

$$\rho(\underline{r}) = \frac{b^{coh.}(\underline{r})}{\Omega(\underline{r})} = \frac{\Sigma_i c_i(\underline{r}) b_i^{coh.}}{\Omega(\underline{r})} \qquad (4.2)$$

b_i^{coh} is the coherent scattering length of the atom i, $c_i(\underline{r})$ its volume fraction, and $\Omega(\underline{r})$ the atomic volume at the position $\underline{r}$. From (4.1) it can be seen that scattering occurs if $\rho(\underline{r})$ is different from $\bar{\rho}$ in the volume of the sample. Differences between $\rho(\underline{r})$ and $\bar{\rho}$ can be caused by regions of different composition (precipitates, voids, shortrange-order) or by regions of different density (dislocations).

Steel contains different kinds of precipitates and also dislocations. In such systems the scattered intensity from different sources is superimposed and cannot a priori be definitely interpreted. In the case of the irradiated steel specimen, the aim was to analyze the irradiation demage. The scattering pattern caused by the irradiation defects could therefore only be determined by subtraction of the scattering curves for the irradiated and the unirradiated specimens. This evaluation procedure assumes that the precipitation structure of the steel does not change during irradiation and annealing. The comparison of the scattering pattern of the annealed and un-

irradiated specimens in Fig. 3.2b shows that such a change does not occur and that the evaluation procedure is therefore correct.

During the neutron irradiation and the subsequent anneal, dislocation loops and voids are produced. Thus, the irradiation induced scattering curves will be interpreted for both types of defects. The scattering law of voids and dislocation loops will be described in the following section.

4.1.1 Scattering Law for Voids

The scattering from voids is caused by the different scattering length densities ρ_P and ρ_M which are the averaged values for voids and matrix. The scattering length density as a function of $\underline{r}$ is

$$\rho(\underline{r}) = \{ \bar{\rho}_p - \bar{\rho} \} \sigma(\underline{r}) + \{ \bar{\rho}_M - \bar{\rho} \} (1 - \sigma(\underline{r})) . \qquad (4.3)$$

$\sigma(\underline{r})$ is equal to one if $\underline{r}$ defines a point within the void, and equal to zero if $\underline{r}$ defines a point within the matrix. The scattering length density for a void is zero and for the matrix is equal to that of iron, to a good approximation. Using (4.3) and (4.1) one obtains for the scattering cross-section

$$\frac{d\Sigma}{d\Omega}(\underline{\kappa}) = \frac{\rho_{Fe}^2}{V_s} \left| \int_{V_s} d\underline{r}\ \sigma(\underline{r})\ e^{i\underline{\kappa r}} \right|^2 . \qquad (4.4)$$

In the case of identical and randomly distributed voids

$$\frac{d\Sigma}{d\Omega}(\underline{\kappa}) = \frac{d\Sigma}{d\Omega}(0) \left| F(\underline{\kappa}) \right|^2 . \qquad (4.5)$$

The cross-section in the forward direction is

$$\frac{d\Sigma}{d\Omega}(0) = \rho_{Fe}^2\, n_p\, v_p^2 = \rho_{Fe}^2\, v_p\, c_p$$

and the formfactor of a void is

$$F(\underline{\kappa}) = \frac{1}{V_p} \int_{V_p} d\underline{r}\, e^{i\underline{\kappa r}} \quad .$$

V_p is the volume of the void, n_p the number of voids per unit volume, and c_p the volume fraction of the voids. The void parameters can be calculated from equs. (4.4) and (4.5). However, there are well established approximate formulas which can very easily be used to calculate the void parameters.

In the small κ-range for $R_g\,\kappa < 1$ the Guinier approximation

$$\frac{d\Sigma}{d\Omega}(\kappa) = \frac{d\Sigma}{d\Omega}(0)\, e^{-(\kappa^2 R_g^2)/3} \qquad (4.6)$$

is valid, where R_g is the Guinier radius. R_g is the second distance moment over the void volume.

$$R_g = \frac{1}{V_p} \int_{V_p} d\underline{r}\, r^2 \qquad (4.7)$$

For a sphere $R_{sph.} = 1.3\, R_g$. R_g can directly be calculated by fitting (4.6) to the experimental curve. The product of void volume and volume fraction can be calculated from the forward scattering.

In the large κ-range for $R_g\,\kappa > 1$ the Porod approximation

$$\frac{d\Sigma}{d\Omega}(\kappa) = P\, \kappa^{-4} \qquad (4.8)$$

$$P = 2\pi\, \rho_{Fe}^2\, n_p\, S$$

with its κ^{-4} dependence is valid for threedimensional particles. From P the averaged area S of a void can be calculated.

A further important quantity in the analysis of the experimental data is the integrated intensity which is an invariant of the

scattering law (4.1).

$$Q = \int_0^\infty d\kappa\ \kappa^2 \frac{d\Sigma}{d\Omega}(\kappa) = 2\pi^2 \rho_{Fe}^2\ c_p\ (1 - c_p) \qquad (4.9)$$

From Q the volume fraction c_p of the voids can be calculated.

4.1.2 Scattering Law for Dislocation Loops

Dislocations produce scattering owing to the long range density changes associated with their strain fields. Taking the atomic volume at a distance $\underline{r}$ from the dislocation core as

$$\Omega(\underline{r}) = \bar{\Omega}\ (1 - \theta(\underline{r}))$$

one obtains to a first approximation the scattering length density

$$\rho(\underline{r}) - \bar{\rho} = \bar{\rho}\ \theta(\underline{r})\ .$$

For a density of n_D dislocations one obtains

$$\frac{d\Sigma}{d\Omega}(\underline{\kappa}) = \rho_{Fe}^2\ n_D |\ \tilde{\theta}(\kappa)|^2 \qquad (4.10)$$

with

$$\tilde{\theta}(\underline{\kappa}) = \int d\underline{r}\ \theta(\underline{r})\ e^{i\underline{\kappa}\underline{r}}\ .$$

Together with

$$\theta(\underline{r}) = -\ \mathrm{Tr}\ \varepsilon_{ij} = -\ \mathrm{div}\ \underline{u}(\underline{r})$$

the straintensor ε_{ij}, and the displacement vector $\underline{u}(\underline{r})$ one also obtains

$$\frac{d\Sigma}{d\Omega}(\underline{\kappa}) = \rho_{Fe}^2\ n_D\ |\ i\underline{\kappa}\ \tilde{\underline{u}}(\underline{\kappa})|^2\ . \qquad (4.11)$$

(4.11) gives the relationship between displacement field and scattering cross-section.

Under the continuum approximation, the cross-section for randomly distributed dislocation loops in an isotropic crystal (a good approximation for polycrystals) is (Seeger and Rühle, 1963)

$$\frac{d\Sigma}{d\Omega}(\underline{\kappa}) = \rho_{Fe}^2 \, n_D \, \left(\frac{1 - 2\nu}{1 - \nu}\right)^2 4\pi^2 \left(\frac{b\,R}{\kappa}\right)^2 \left\langle \left(\frac{\kappa}{\kappa} J_1(\kappa R)\right)^2 \right\rangle . \qquad (4.12)$$

ν is the Poisson constant, $\underline{b}$ the Burgers vector, $\underline{R}$ the radius of the loop, and J_1 the Bessel function of first order.

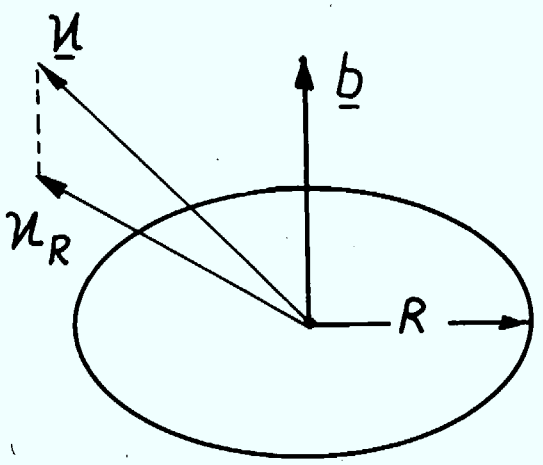

Fig. 4.1 Dislocation loop with Burgers vector $\underline{b}$ and radius $\underline{R}$. κ_R is the projection of $\underline{\kappa}$ onto the area of the dislocation loop.

Using Guinier's approximation (4.6) one obtains from (4.12) the Guinier radius $R_g = 0.8\ R$ and the scattering cross-section in forward direction

$$\frac{d\Sigma}{d\Omega}(0) = \rho_{Fe}^2 \, n_D \, \left(\frac{1 - 2\nu}{1 - \nu}\right)^2 \frac{8\pi^2}{15} b^2 \, R^4 . \qquad (4.13)$$

From the Guinier radius one obtains the radius of the dislocation loop, and from the cross-section in the forward direction their density n_D.

In the large κ-region Porod's approximation is applicable. It has a κ^{-3} dependence.

$$\frac{d\Sigma}{d\Omega}(\kappa) = P'\kappa^{-3}$$

$$P' = \rho_{Fe}^2 \, n_D \, (\frac{1 - 2\nu}{1 - \nu})^2 \, \pi^2 \, b^2 \, R \qquad (4.14)$$

From this formula new parameters cannot be calculated. However, it can be used to prove the consistency of the parameters calculated from (4.13). Furthermore, if the experimental results have a κ^{-3} dependence one can exclude the existence of voids.

4.2 Analysis Procedure for Steel A

Guinier and Porod plots are shown in Figs. 4.2a-c and 4.3a-c for the irradiation induced scattering of steel A directly after irradiation, and after the first and second anneals. In a Guinier plot cross-section and scattering vector are plotted on a logarithmic and a quadratic scale respectively. For such a plot Guinier's approximation (4.6) yields a straight line. As can be seen from the straight line fitted to the experimental points in Figs. 4.2a-c, a Guinier region exists for all three curves. The slope of the straight lines gives the Guinier radius and their extrapolation to $\kappa = 0$ the scattering cross-section in the forward direction. These values are shown in the figures.

In a Porod plot the cross-section and the scattering vector are both plotted on logarithmic scales. The cross-section of a void (4.8) yields a straight line with a slope of -4 and the cross-section of a dislocation loop (4.14) yields a straight line with a slope of -3. For the spectrum of the annealed sample no Porod region (Fig. 4.3a) exists. This means that this scattering curve cannot only be interpreted by dislocation loops or voids having $R_g \kappa > 1$. Therefore, the measurements have to be extended to larger κ-values in order to obtain further quantitative results about the defect structure of the unannealed sample.

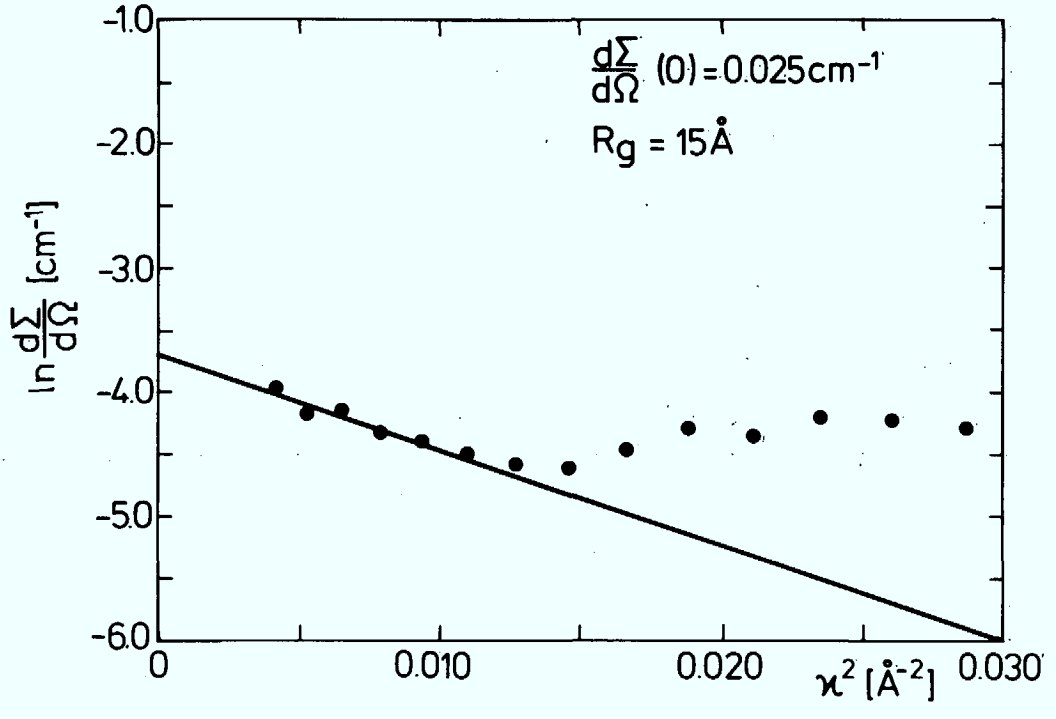

Fig. 4.2a

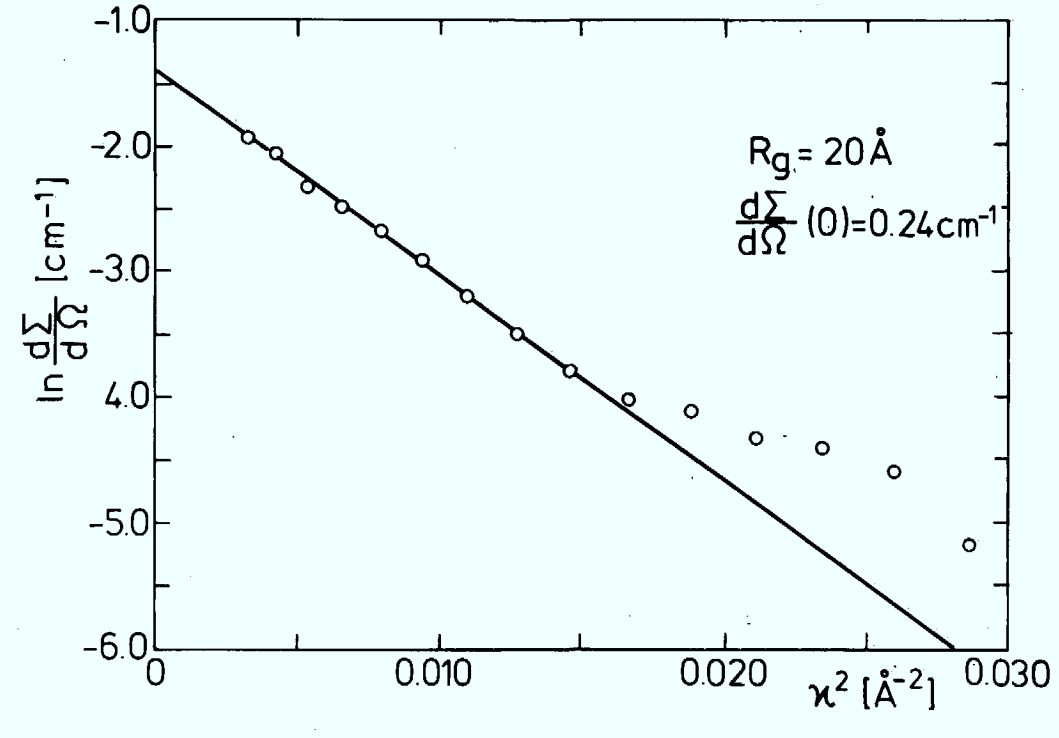

Fig. 4.2b

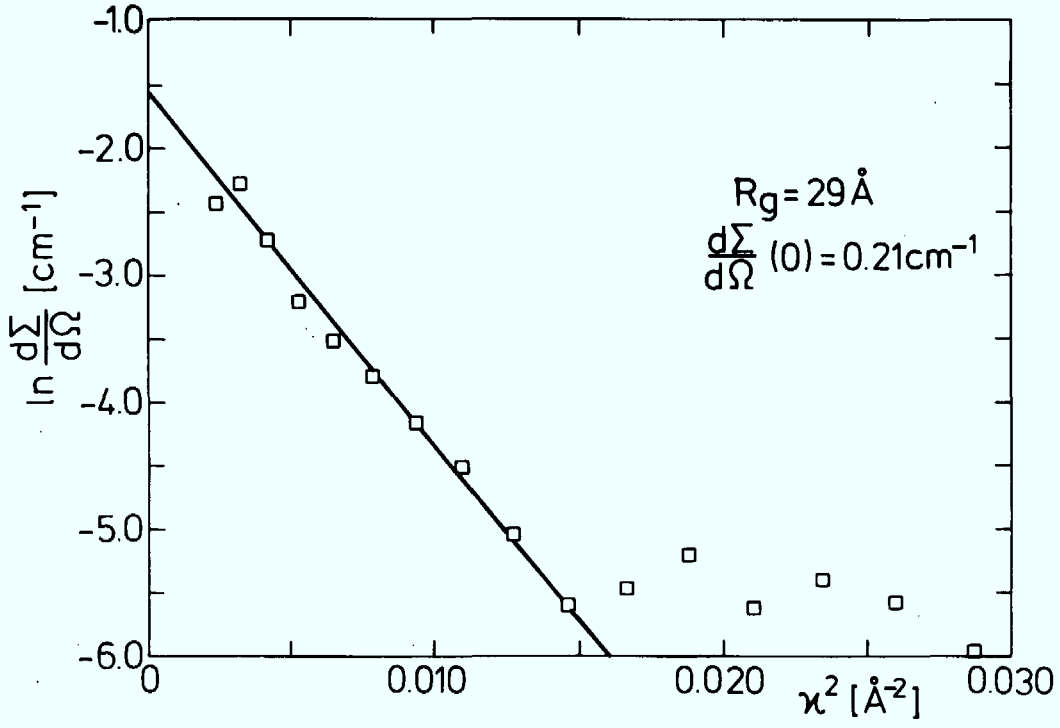

Figs. 4.2a-c Guinier plot of the irradiation induced scattering of steel A.

a) Without annealing,

b) after the first anneal at 300°C, and

c) after the second anneal at 350°C.

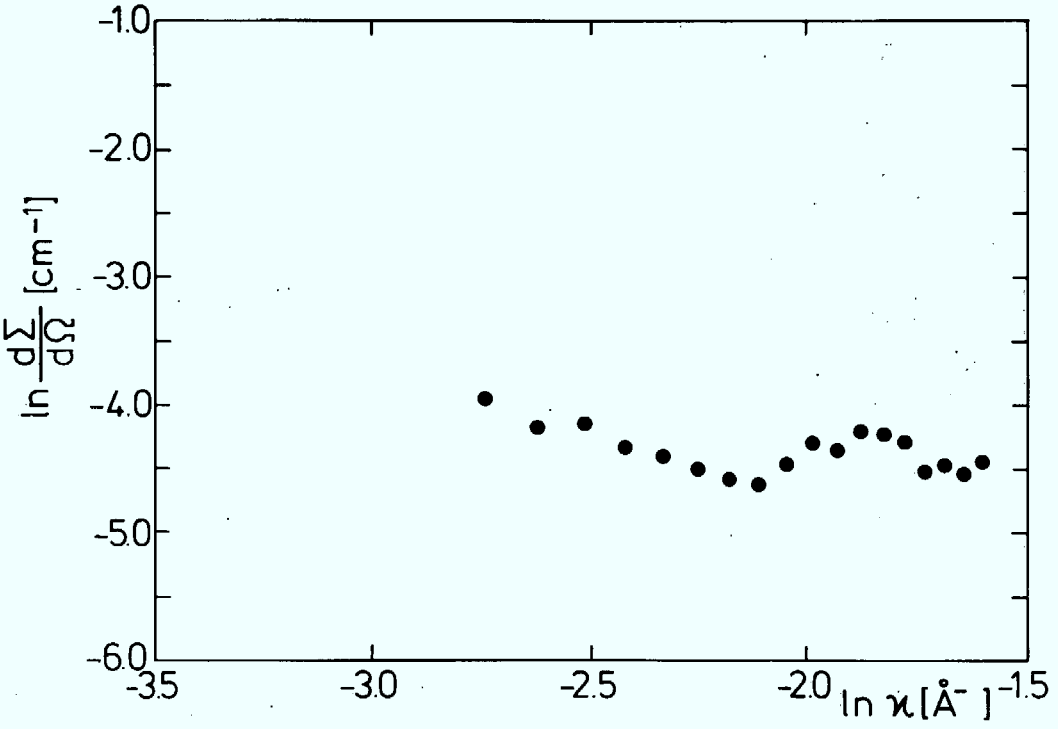

Fig. 4.3a

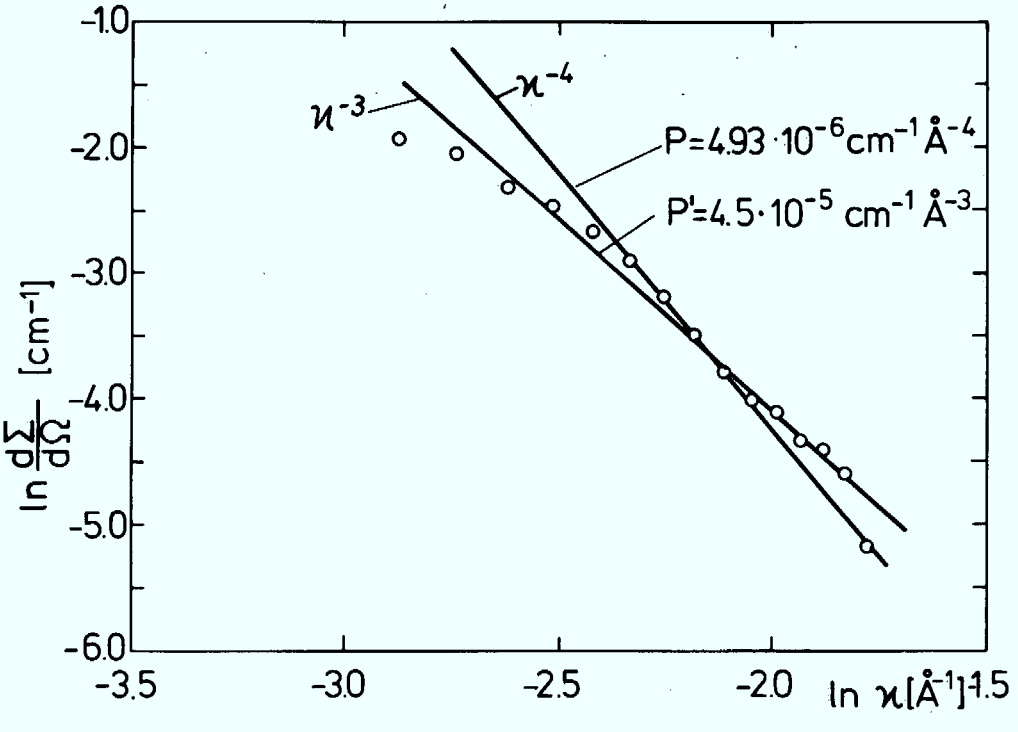

Fig. 4.3b

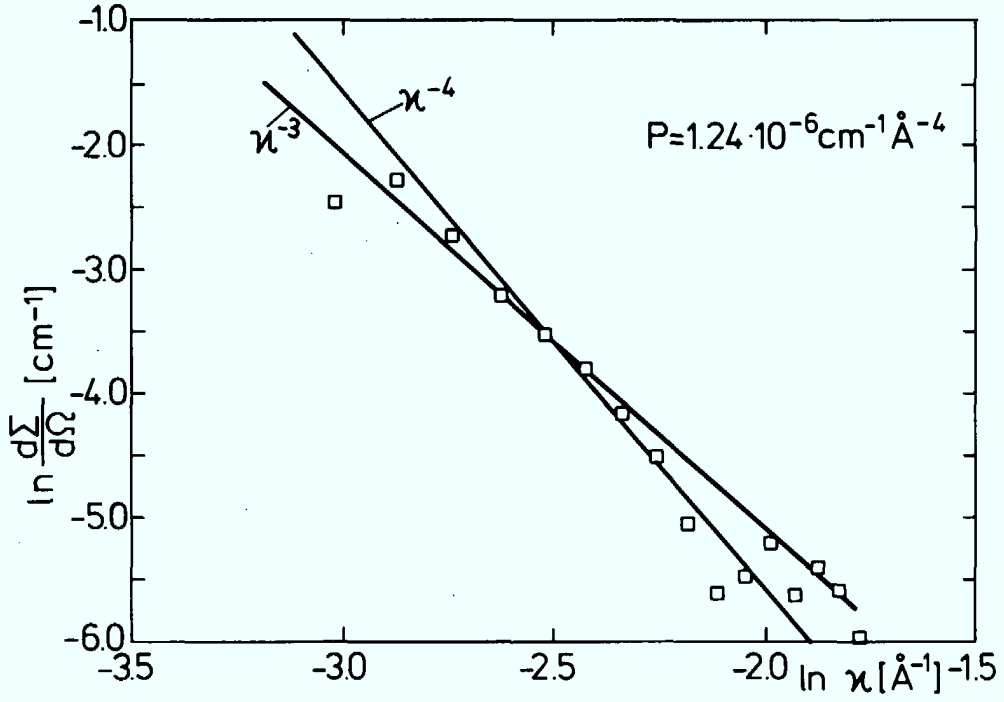

Figs. 4.3a-c Porod plot of the irradiation induced scattering of steel A (see text of Figs. 4.2a-c).

After the first and second anneals a Porod region exists, as can be seen from Figs. 4.3b and c, where straight lines of slope -4 and -3 are fitted to the experimental points. Undoubtedly, a Porod region with a slope of -4 (Fig. 4.3c) exists for the specimen after the second anneal, whereas for the first anneal (Fig. 4.3b) a decision between a slope of -4 and -3 cannot clearly be made.

4.3 Results for Steel A

4.3.1 Void Parameters

Assuming voids produce the scattering, parameters calculated from the experimental data are contained in Tab. 4.1. For the first and second anneals all obtainable parameters could be calculated; whereas for the unannealed sample no Porod behaviour

Calculated from	unannealed	1 x annealed at 300°C for 4h	2 x annealed at 350°C for 4h	statistical error
Q	–	$C = 5 \cdot 10^{-4}$	$C = 1.9 \cdot 10^{-4}$	± 10 %
Slope in Guinier region	$R_g = 15$ Å	$R_g = 20$ Å	$R_g = 29$ Å	± 5 %
R_g	$v_p = 3 \cdot 10^4$ Å^3 $D = 39$ Å	$v_p = 7.4 \cdot 10^4$ Å^3 $D = 52$ Å	$v_p = 22.4 \cdot 10^4$ Å^3 $D = 75$ Å	± 15 %
$\frac{d\Sigma}{d\Omega}(o)$ / Q	—	$v_p = 5.6 \cdot 10^4$ Å^3 $D = 47$ Å	$v_p = 13.1 \cdot 10^4$ Å^3 $D = 63$ Å	± 18 %
Q, $\frac{d\Sigma}{d\Omega}(o)$	——	$n_p = 9 \cdot 10^{15}$ cm^{-3}	$n_p = 1.5 \cdot 10^{15}$ cm^{-3}	± 25 %
p, $\frac{d\Sigma}{d\Omega}(o)$ Q	——	$S = 1.03 \cdot 10^4$ Å^2 $D = 57$ Å	$S = 1.7 \cdot 10^4$ Å^2 $D = 74$ Å	± 25 %
R_g, $\frac{d\Sigma}{d\Omega}(o)$	$n_p = 1.3 \cdot 10^{15}$ cm^{-3} $R_g = 15$ Å	——	——	

Tab. 4.1 Void parameters for steel A.

could be found because of experimental limitations.

The volume fraction c_p of the voids is calculated from the integrated intensity Q (4.9). Q is calculated by integrating over the total κ-region using the experimental and the extrapolated Guinier and Porod curves.

$$Q = 8.4\ 10^{-5}\ \text{Å}^{-3}\ \text{cm}^{-1} \quad \text{for 1st anneal}$$

$$Q = 3.1\ 10^{-5}\ \text{Å}^{-3}\ \text{cm}^{-1} \quad \text{for 2nd anneal.}$$

In order to calculate the scattering length density, the nuclear and magnetic scattering lengths had to be considered. Using $b_{Fe}^{nuc.} = 0.96\ 10^{-12}$ cm, $b_{Fe}^{mag.} = 0.6\ 10^{-12}$ cm (Bacon, 1967), $v_c = 11.7$ Å^3 (Pearson, 1967), and

$$\rho_{Fe}^2 = \frac{(b_{Fe}^{nuc.})^2 + 2/3(b_{Fe}^{mag.})^2}{\Omega^2} \qquad \text{(Bacon, 1967)}$$

one obtains $\rho_{Fe}^2 \doteq 85\ 10^{20}\ \text{cm}^{-4}$. c_p is identical to the swelling volume, which is a very important parameter for the characterization of irradiation effects. The value ρ_{Fe}^2 is only necessary for the evaluation of the volume fraction. In the calculation of the other parameters ρ_{Fe}^2 cancels out, as can be seen from the formulas in 4.1.1.

Considering the void parameters in Tab. 4.1 for the first and second anneals, the following picture emerges. The volume fraction has decreased during the second anneal of 350°C from $5\ 10^{-4}$ to $1.9\ 10^{-4}$. The average diameter of the voids, which agrees from three independent calculations, has increased from about 50 ot 70 Å and the particle density n_p has decreased from $9\ 10^{15}\ \text{cm}^{-3}$ to $1.5\ 10^{15}\ \text{cm}^{-3}$. These values are reasonable if one compares them with the TEM-measurements of Smidt and Sprague (1973). For irradiated iron ($\phi = 4.5\ 10^{20}\ \text{n/cm}^2$, $E > 1$ MeV, 280°C) alloyed with 0.3 at% Cu, Ni or C, these authors found void diameters between 29 and 51 Å and densities of

about 10^{15} cm^{-3}. Thus the comparison of these experimental results with ours gives an important indication that, essentially, voids produce the scattering.

4.3.2 Dislocation Loop Parameters

Assuming that only dislocation loops are present, the results obtained from the scattering curves are summarized in Tab. 4.2. The loop diameter is calculated from the Guinier radius and the loop density from the Guinier radius and the cross-section in the forward direction (4.13). The Burgers vector is equal to $b = 2.5$ Å ($b = (\sqrt{3}/2)a$, a is the lattice parameter), the Poisson ratio $\nu = 0.38$, and the square of the nuclear scattering length density $\rho^2_{Fe} = 67\ 10^{20}$ cm^{-4}. The nuclear scattering length density is used because the magnetic scattering from dislocations has a different κ-behaviour than for their nuclear scattering (Schmatz et al., 1974). The magnetostriction causes long range correlations of the magnetization field around a dislocation

calculated from	unannealed	1 x annealed	2 x annealed	
slope in Guinier region	$R_g = 15$ Å	$R_g = 20$ Å	$R_g = 29$ Å	± 5 %
R_g	$D = 38$ Å	$D = 50$ Å	$D = 72$ Å	± 5 %
$\frac{d\Sigma}{d\Omega}(o), R_g$	$n_D = 2.4\ 10^{18}$ cm^{-3}	$n_D = 1.9\ 10^{19}$ cm^{-3}	$n_D = 3.7\ 10^{18}$ cm^{-3}	
P', R_g	-	$n_D = 3\ 10^{19}$ cm^{-3}	-	

Tab. 4.2 Dislocation loop parameters for steel A.

which means that the magnetic dislocation scattering is concentrated in the small κ-region. If we compare the results, assuming pure dislocation loop scattering, with the TEM results of Smidt and Sprague (1973) the calculated diameters of the loops are in a fairly good agreement. However, the calculated densities are two to three orders of magnitude too high. Smidt and Sprague measured diameters between 40 - 60 Å and densities of 10^{15} - 10^{16} cm^{-3}. Furthermore, if one calculates the average separation of the loops from their densities, one obtains values which are smaller than their diameter. For physical reasons, the loops should become unstable at the annealing temperatures and also interparticle interference effects should have influenced the measured curves.

4.4 Results for Steel B and Weld Material

The irradiation induced cross-sections for the unannealed steel B and weld material are shown in a Guinier plot in Figs. 4.4 and 4.5. Both curves are qualitatively equal to the curve for steel A in the unannealed state (Fig. 4.2a). The cross-sections have the average value:

$$\left.\frac{d\Sigma}{d\Omega}\right|_{\text{Steel A}} = 0.015\ cm^{-1}, \qquad \left.\frac{d\Sigma}{d\Omega}\right|_{\text{Steel B}} = 0.0043\ cm^{-1}$$

$$\left.\frac{d\Sigma}{d\Omega}\right|_{\text{Weld Mat.}} = 0.009\ cm^{-1}$$

These cross-sections are produced by defects having a Guinier radius smaller than or equal to 5 Å, as can be seen from the straight lines in Fig. 4.4. If it is assumed that the defects have the same average volume in all three systems, one finds that steel A contains 3.5 times as many defects as steel B. The weld material contains 2.1 times as many.

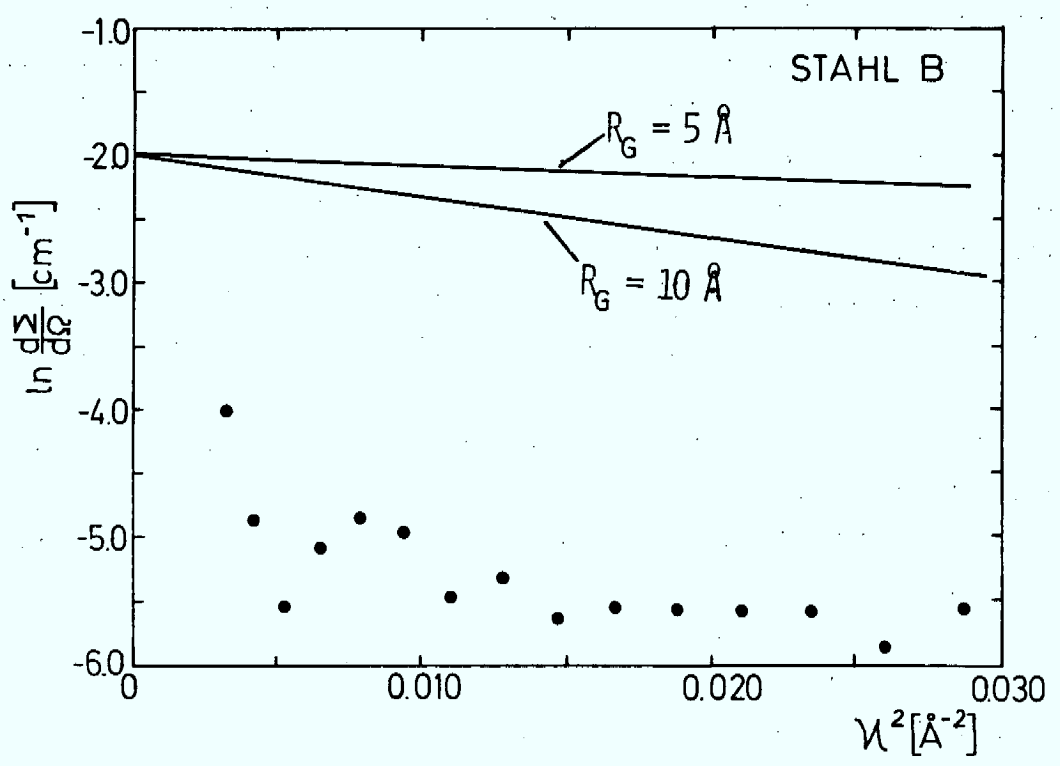

Fig. 4.4 Guinier plot of the irradiation induced scattering of steel B.

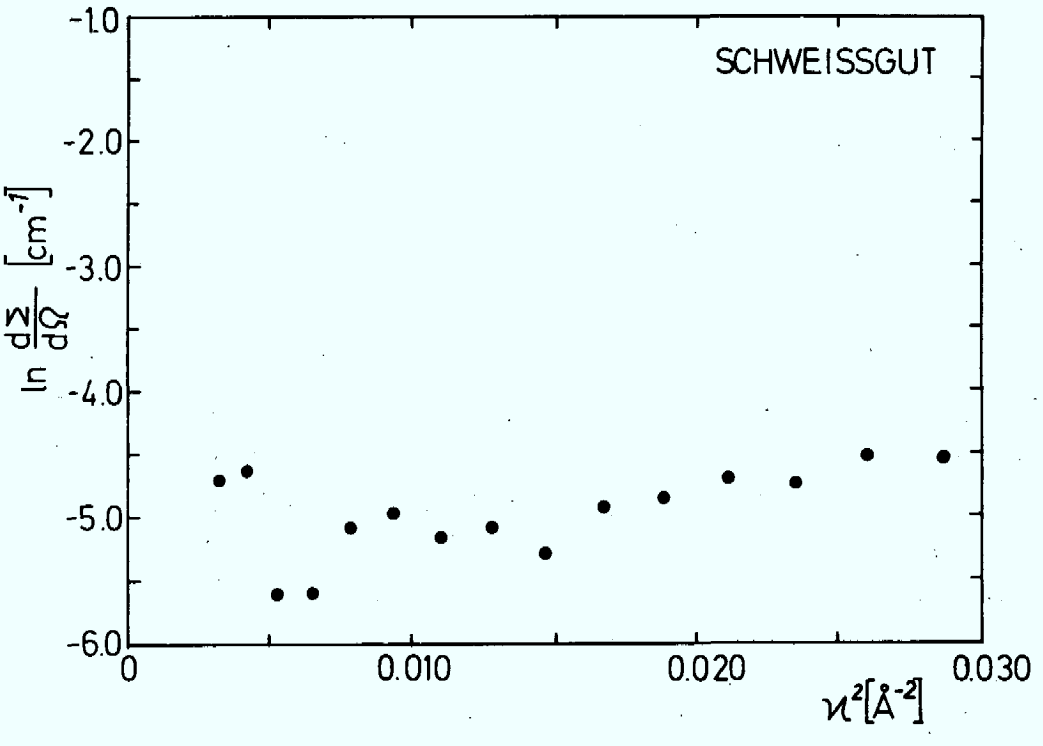

Fig. 4.5 Guinier plot of the irradiation induced scattering of the weld material.

5. Discussion

Three different steel systems having a 50 % enhancement of irradiation induced hardness were measured using neutron small angle scattering. The strongest scattering effect was found in steel A; the standard reactor containment steel material ASTM A 533 B. This system was irradiated with a neutron fluence of $7\ 10^{19}$ n/cm^2 (E > 1 MeV) at a temperature of 150°C. For this specimen, neutron scattering spectra were also measured after isochronal anneals (4 hours) at 300, 350, 400, and 450°C.

The irradiation induced scattering curves were interpreted by two different models. For the first model it was assumed that only voids produce the scattering and in the second model that only dislocation loops produce the scattering. The scattering curves were evaluated using well established scattering formulas, i.e. the Guinier and Porod approximations. Assuming voids, consistent values were obtained from the scattering curves which are in fairly good agreement with TEM studies carried out by Smidt and Sprague (1973) on similarly prepared dilute iron alloys. The consistency of our calculations was proved by calculating the diameter of the voids from three independent parameters given by the scattering curves. The agreement between the TEM results and ours, assuming dislocation loops, could not be shown. In our calculations dislocation loop densities of 10^{18} - 10^{19} cm^{-3} were obtained, which are two to three orders of magnitude higher than those measured in the TEM experiments. Furthermore, the distance between the dislocations is smaller than their diameter. Physically, this means that the dislocation loops become unstable at the annealing temperatures and also interference effects between the closely spaced dislocation loops should be seen in the scattering experiment. From these arguments we believe that our measured scattering curves are caused by voids. Dislocation loops with a density of 10^{15} - 10^{16} cm^{-3}, as seen in TEM studies, cannot be measured since the scattering produced by voids of similar diameter and density is two orders of magnitude higher. However, TEM results would be useful for a clear interpretation of the neutron scattering spectra.

Up to now, no annealing experiments have been done with the weld material whereas for steel B, after annealing from 50 to 32 % hardness enhancement, no voids with a diameter larger than 20 Å were observed (Fig. 3.3a). Steel B has a vanadium content of 0.2 wt. %. This result is in agreement with the above mentioned TEM studies where no voids were seen in the 0.3 at% vanadium and iron alloy.

Next, the anneal of hardness enhancement for steel A in Fig. 2.1 is compared with the neutron scattering spectra (Figs. 3.2a,b, 4.2a-c, 4.3a-c). The hardness enhancement of 50 % produced by irradiation decreased during the first anneal at 300°C to 30 % and during the second anneal at 350°C to 18 %.
The neutron scattering spectra show that during the first and second anneal voids with $R_g < 5$ Å (Fig. 4.2a) vanished continuously. This can be seen from the tail of the curves in Figs. 4.2b and c. As shown in Figs. 4.2a-c, these voids have coagulated into larger voids which are measured in the Guinier region and have vanished during annealing. The decrease of hardness enhancement from 18 % to zero during subsequent anneals is not accompanied by a detectable change in the scattering pattern. The scattering patterns for these anneals were identical to the pattern for the unirradiated specimen within statistical error.

The scattering intensities of all three systems after irradiation (Figs. 4.2a, 4.4, and 4.5), which all had the same amount of irradiation induced relative hardness enhancement, are different. The ratios of their average intensities are

$$\frac{\left\langle \frac{d\Sigma}{d\Omega} \right\rangle_{\text{Steel A}}}{\left\langle \frac{d\Sigma}{d\Omega} \right\rangle_{\text{Steel B}}} = 3.5 \quad \text{and} \quad \frac{\left\langle \frac{d\Sigma}{d\Omega} \right\rangle_{\text{Steel A}}}{\left\langle \frac{d\Sigma}{d\Omega} \right\rangle_{\text{Weld Mat.}}} = 1.7 \; .$$

These are approximately equal to the ratios of the fluences, i.e.

$$\frac{\phi_{\text{Steel A}}}{\phi_{\text{Steel B}}} = 4.7 \quad \text{and} \quad \frac{\phi_{\text{Steel A}}}{\phi_{\text{Weld Mat.}}} = 1.4 \; .$$

To determine a proportional relationship between the forward scattering of the unannealed specimens and the neutron fluence more neutron scattering experiments are necessary. In particular, the measurements have to be extended to larger κ-values in order to obtain reliable information on small defects.

Finally, it was successfully shown that quantitative information on irradiation induced defects in reactor pressure vessel steel is obtainable using the small angle neutron scattering technique. The experiments described above should be the basis for future systematical investigations of irradiated steel.

Acknowledgments

We would like to thank Mr. G. Pohl for his help with the neutron scattering experiments, also Mr. H. Derz and his collegues in the Hot Cells Department for preparing the irradiated specimens, and Dr. R. Beddoe for carefully reading the english manuscript.

Literature

Bacon, G.E. (1967), "Neutron Diffraction", At the Clarendon Press, Oxford

Frisius, F. and Naraghi, M. (1977), Atomkernenergie 29, 139

Guinier, A. and Fournet, G. (1955), "Small Angle Scattering of X-Rays", John Wiley, New York

Pachur, D. (1975), IAEA-Report 176,

Pachur, D. and Sievers, G. (1975), Stahl und Eisen 95, 45

Pachur, D. (1976), Arch. Eisenhüttenwesen 47, 501

Pearson, W.B. (1967), "Handbook of Lattice Spacings and Structures of Metals and Alloys", Pergamon Press, Oxford

Schelten, J. (1972), Kerntechnik 14, 86

Schmatz, W., Springer, T., Schelten, J., and Ibel, K. (1974), J. Appl. Cryst. 7, 96

Seeger, A. and Rühle, M. (1963), Annalen der Physik 11, 217

Smidt, F.A.,Jr. and Sprague, J.A. (1973), ASTM STP 529 American Society for Testing and Materials, p. 78